Electrochimica Acta 202 (2016) 203–208

Contents lists available at ScienceDirect

Electrochimica Acta

journal homepage: www.elsevier.com/locate/electacta

Hierarchical rutile TiO_2 with mesocrystalline structure for Li-ion and Na-ion storage

Zhensheng Hong[a,b,*], Jiaxing Hong[a], Chaobing Xie[a], Zhigao Huang[a,b], Mingdeng Wei[c,*]

[a] College of Physics and Energy, Fujian Normal University, Fujian Provincial Key Laboratory of Quantum Manipulation and New Energy Materials, Fuzhou 350117, China
[b] Fujian Provincial Collaborative Innovation Center for Optoelectronic Semiconductors and Efficient Devices, Xiamen 361005, China
[c] State Key Laboratory of Photocatalysis on Energy and Environment, Fuzhou University, Fuzhou, Fujian 350002, China

ARTICLE INFO

Article history:
Received 8 December 2015
Received in revised form 4 April 2016
Accepted 5 April 2016
Available online 6 April 2016

Keywords:
TiO_2
mesocrystalline structure
lithium-ion batteries
sodium-ion batteries
anode

ABSTRACT

In this paper, we report a one-step and additive-free route for synthesizing hierarchical rutile TiO_2 with mesocrystalline structure. The rutile TiO_2 architecture constructed by oriented tiny nanorod subunits (around 5 nm in diameter) have nano/submicro hierarchical structures, nanoporous nature, a relatively large surface area and high tapped density. When the hierarchical rutile TiO_2 was studied as anode material for Li-ion batteries (LIBs), they exhibited a high reversible capacity of more than 250 mAh g^{-1} within a voltage window of 1–3 V, superior rate capability and very good cycling stability with 220 mAh g^{-1} after 100 cycles at 0.1 A g^{-1}. It's notable that the hierarchical rutile TiO_2 exhibited superior Li-ion storage properties under deep cycling conditions (0.01-3.0 V), a stable capacity of 346 mAh g^{-1} after 100 cycles at 0.1 A g^{-1} could be remained. The hierarchical TiO_2 also displayed a large reversible capacity of more than 255 mAh g^{-1} (average value) at 0.05 A g^{-1} and good cycling performance for Na-ion insertion. These results, in combination with high volumetric storage capacity, render hierarchical rutile TiO_2 a promising anode material for rechargeable batteries.

1. Introduction

Lithium-ion batteries (LIBs) remain the most prominent rechargeable energy storage and conversion technology due to the significant importance for the portable electronics, communication facilities and rapidly growing sector of environmentally benign electric vehicles (EVs) [1–4]. Recently, sodium-ion batteries (NIBs) with identical conception have attracted great interest because Na is a more abundant alkali metal element as well as more evenly distributed compared to Li [5–7]. Developing anode (negative) materials for LIBs and NIBs with high performance is receiving high level of scientific attention [7,8]. In the past few years, metal oxides have been considered as promising alternative anode candidates for LIBs [8]. With regard to NIBs, a major obstacle in realizing them is the absence of efficient anode materials [7].

Titanium dioxide (TiO_2) with multiple polymorphs (e.g., anatase, rutile, brookite, TiO_2-B) has been utilized as an electrochemical energy storage material such as in LIB and NIB anodes due to their high rate performance, good cycling stability, intrinsic safety, low cost and environmental friendliness compared to other anode materials [9–12]. However, the electrochemical performances of pristine TiO_2 are relatively poor due to its poor electrical conductivity and low ion diffusion coefficients, which limit its application in high power/energy density energy storage devices [9,13]. In general, the electrochemical properties of TiO_2 largely depend on its crystalline phase, size, surface state and microstructures [9,10]. Among the multiple polymorphs of TiO_2, rutile TiO_2 appeared special that its Li-ion storage properties largely depend on the size, and Li-ion nearly can't insert into microsized rutile structure [14]. It's also notable that the rutile TiO_2 exhibited good Li-ion storage performance in an enlarged potential window (0.1–3 V) [15]. To tailor the properties of TiO_2, many strategies have been adopted to design TiO_2 nanostructures with various morphologies, such as one-dimensional nanowires and nanotubes, two-dimensional nanosheets and three-dimensional (3D) architectures or mesoporous structures [16–22]. Although they exhibited improved storage capacity due to the nanosized advantage, many of them suffered from low tapped density.

Most recently, mesocrystals, a class of new solid materials, have attracted a great deal of research interests in the applications for energy storage and conversion [23–25]. Initially, the concept of

* Corresponding authors. Tel.: +86 591 22868132; fax: +86 591 22868132.
E-mail addresses: winter0514@163.com (Z. Huang), wei-mingdeng@fzu.edu.cn (M. Wei).

http://dx.doi.org/10.1016/j.electacta.2016.04.017
0013-4686/

"mesocrystal" was proposed by Cölfen and Antonietti in 2005 based on the studies of the structures and formation mechanisms of biominerals and their mimetics. Mesocrystals, being colloidal in composition, are built by individual nanocrystal subunits with crystallographically oriented directions, leading to a "single-crystal-like" electron diffraction spots [23]. It's demostrated that mesocrystals have been studied for enhancing the discharge capacity and reaction kinetics in LIBs, owing to their unique combination of nanosized advantage and order over a microscopic size regime [26,27]. Such highly oriented assemblies possess nanoporous nature and single-crystal-like structure, which provide the efficient lithium-ion insertion/extraction reaction, and short distance for charge transport.

In this study, we report a one-step, additive-free and facile route for synthesizing hierarchical rutile TiO_2 with mesocrystalline structure. The hierarchical rutile TiO_2 possesses nano/submicro hierarchical structures, nanoporous nature and high tapped density. When evaluated as an anode material for LIBs and NIBs, it exhibited a high reversible capacity, improved initial Coulombic efficiency, superior rate capability, and very good cycling stability compared to commercial TiO_2 nanoparticles.

2. Experimental

2.1. Materials Synthesis

The hierarchical rutile TiO_2 with mesocrystalline structure (TiO_2-HMs) was prepared through a one-step synthetic route under a low temperature. In a typical synthesis, 1.5 mL of titanium (IV) isopropoxide (TIP) was dropped into 50 mL 2.2 M HCl solution, and then kept at 80 °C for 48 h under stirring. The final white product was obtained by centrifugation, washed with distilled water for several times to remove the residual inorganic ions and dried at 60 °C for 12 h. The chemicals were purchased from Aladdin company.

2.2. Characterizations of the samples

X-ray diffraction (XRD) patterns were obtained on a PANalytical X'Pert diffractometer using the Co Kα radiation (λ = 1.78897 Å), and then the data were converted to Cu Kα data through a standard XRD data (Cu) transformation performed by X'Pert HighScore software. Scanning electron microscopy (SEM, S8010 instrument) and transmission electron microscopy (TEM, FEI F20 S-TWIN instrument) were performed for the morphological and structural characterization of the obtained samples. N_2 adsorption–desorption analysis was measured on a Micromeritics TriStar II 3020 instrument (USA). The pore size distributions of the as-prepared samples were analyzed using Barrett Joyner Halenda (BJH) methods.

2.3. Electrochemical Measurements vs. Li and Na

The active materials dried at 120 °C for 12 h in a vacuum oven were admixed with super-P (SCM Industrial Chemical Co.Ltd.) and polyvinylidene fluoride (PVDF, SCM) binder additive in a weight ratio of 70:20:10. The mixture was spread and pressed on circular copper foils as working electrodes (WE), and dried at 120 °C in vacuum for 12 h. Li-ion cells were assembled in coin-type cells (CR 2025) with a Li metal foil (Taiyuan Source of Lithium Technology Center) as the negative electrode, a polypropylene separator (Celgard 2400), and 1 M $LiPF_6$ in a 1/1/1 (volume ratio) mixture of ethylene carbonate (EC), ethylene methyl carbonate (EMC) and dimethyl carbonate (DMC) as the electrolyte (Zhangjiagang Guotai-Huarong New Chemical Materials Co.Ltd.). Na-ion cells were also assembled in coin-type cells (CR 2025) with a Na metal foil (Aladdin) as the negative electrode, glass fiber separator (Whatman GF/F), and 1 M $NaClO_4$ in EC and diethyl carbonate (DEC) (1/1 in volume) as the electrolyte. The cells were assembled in a glove box filled with highly pure argon gas (O_2 and H_2O levels < 1 ppm), and charge/discharge tests were performed on a Land automatic batteries tester (Land CT 2001A, Wuhan, China). Cyclic voltammetry (CV) measurements were performed on Zennium (Zahner). For the charge/discharge tests of Li-ion batteries within the voltage window of 0.01–3 V vs. Li/Li^+, the cells were activated by 5 cycles at 0.1 A g^{-1} in the voltage window of 1–3 V. The electrochemical impedance spectroscopy (EIS) was also performed on Zennium electrochemical workstation with an AC voltage amplitude of 5 mV in the frequency range from 1 MHz to 100 mHz.

3. Results and discussion

The hierarchical rutile TiO_2 (TiO_2-HMs) was fabricated by a one-step and addtive-free synthetic route. Fig. 1a shows the X-ray diffraction (XRD) patterns of as-prepared TiO_2-HMs. All the diffraction reflections could be indexed to tetragonal rutile TiO_2 (JCPDS 65-0191) and no reflections related to impurity phases were found. The broadened diffraction reflections indicate a small crystallite size of the sample. The average crystallite size of TiO_2-HMs was calculated to be approximately 12 nm, using the Scherer equation, based on the (110) diffraction peak. N_2 adsorption–desorption isotherms measurements were utilized to characterize the Brunauer-Emmett-Teller (BET) surface area and pore size distribution, as presented in Fig. 1b. The BET surface area and the pore volume of TiO_2-HMs were determined to be 62 $m^2 g^{-1}$ and 0.14 $cm^3 g^{-1}$, respectively. Fig. 1b (inset) shows the pore size distribution of TiO_2-HMs, such material exhibits a relatively narrow size distribution of mesopores (aroud 3.4 nm) caculated by the BJH methods. On the other hand, the BET surface area of commercial rutile TiO_2 nanoparticles (TiO_2-NPs) was about 34 $m^2 g^{-1}$, which did not show mesoporous structure.

The morphology of TiO_2-HMs obtained from HCl solution was characterized by scanning electron microscopy (SEM) and

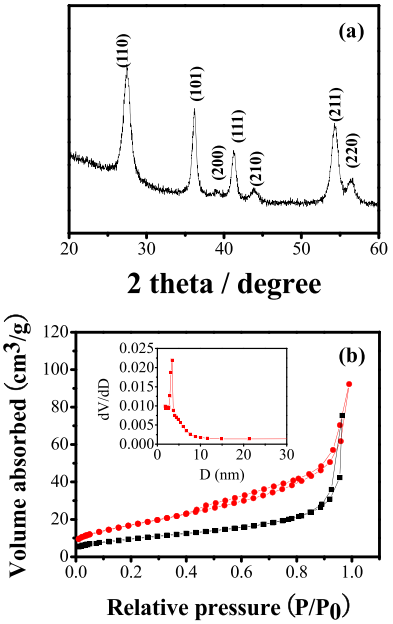

Fig 1. (a) XRD pattern and (b) N_2 adsorption–desorption isotherm of the hierarchical rutile TiO_2 (TiO_2-HMs) and commercial rutile TiO_2 nanoparticles (TiO_2-NPs). The inset in (b) is the corresponding BJH pore size distribution of TiO_2-HMs.

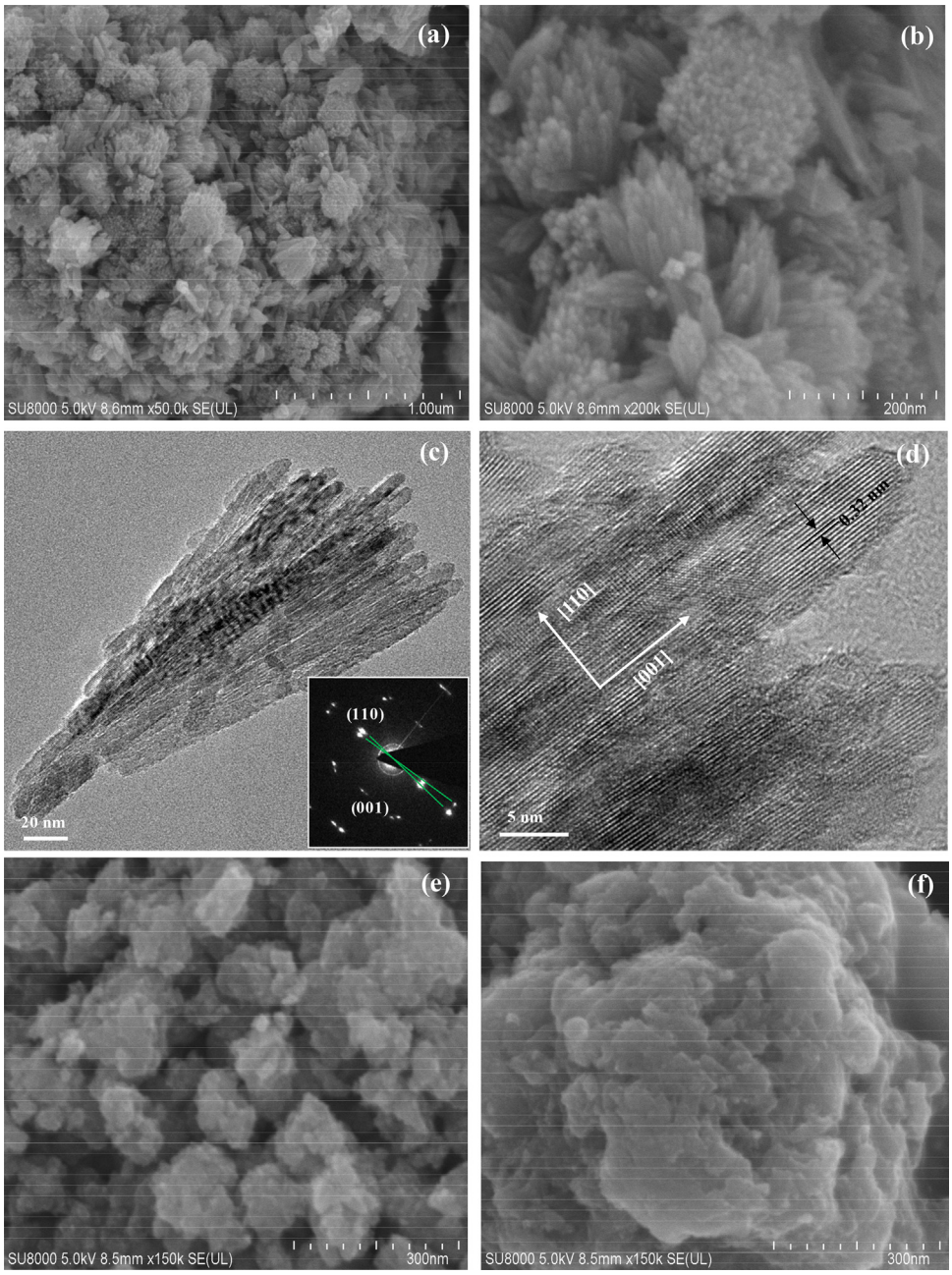

Fig. 2. (a-b) SEM, (c) TEM and (d) HRTEM images of TiO_2-HMs obtained from HCl solution, SEM images of the samples obtained from HNO_3 (e) and H_2SO_4 (f) solutions. The inset in (c) is the related SAED pattern.

transmission electron microscopy (TEM), the results are shown in Fig. 2. It is observed from the SEM images (Fig. 2a and Fig. 2b) that numerous bundle-like products with length about several hundred nanometers were formed. It's interesting that such bundle-like products are connected and interlaced with each other. It should be pointed out that every single bundle was composed of tiny nanorods. Fig. 2c displays typical TEM image of a single bundle, which confirms that the bundle-like product was constructed by tiny nanorod subunits. The corresponding SAED pattern for the whole bundle shown in the inset of Fig. 2c exhibited a single-crystal-like diffractions, indicating that the building of nanorod subunits were highly ordered, and thus resulting to the formation of crystallographic oriented mesocrystalline structure. However, the diffraction spots were elongated and it could be observed that the bundle-like material along the [110] direction have two sets of adjacent diffraction spots. This result suggests that there was a relatively large mismatch between the boundaries of the nanorod subunits when they were assembled into the loosely packed bundle-like products. Such phenomenon was usually found for the mesocrystals which were formed through oriented attachment route [23–25]. Moreover, the hierarchical rutile TiO_2 constructed by nanorod subunits with diameter around 5 nm was highly crystallized, as revealed from the HRTEM image in Fig. 2d. The clear lattice fringe of 0.32 nm was assigned to the (110) spacing of rutile structure. It's worth mentioning that the rutile TiO_2 nanorods growing along [001] direction could maximize Li storage because the channel along the c-axis is known to be a "highway" for Li transport due to the lowest energy barrier [28,29].

It's interesting that the hierarchical rutile TiO_2 cannot be formed when the reaction solution were replaced with HNO_3 or H_2SO_4 aqueous solution. As shown in the SEM images (Fig. 2e and Fig. 2f), only aggregate nanoparticles were found in the above two

reaction solution. Thus, the anion had a remarkable effect on the microstructures of the final product in this reaction system. This phenomenon was also found and discussed in our previous study on the controllable synthesis of TiO_2 mesocrystals [30]. In fact, it's demonstrated that Cl^- had a lower binding energy to the (001) surface of the rutile TiO_2 nuclei, leading to the formation of rutile TiO_2 nanocrystals with anisotropic morphology [29]. However, mesocrystalline rutile TiO_2 were not formed in HNO_3 aqueous solution in this study. This may be due to the larger steric block effect or larger binding energy for NO_3^- on TiO_2 nuclei, which may be not good for the appearance of oriented attachment of nanocrystals. Therefore, the 3D hierarchical superstructures assembled by rutile TiO_2 nanorods growing along [001] direction were preferably formed in HCl solution.

Recently, crystallographically oriented nanoparticle superstructures (mesocrystals) exhibited promising applications as electrode materials for lithium-ion batteries [26,27,30]. Such a new class of ordered assemblies provides some unique advantages, such as the structural stability of microsized electrodes while exploiting the beneficial properties associated with nanosized electrodes. Herein, the hierarchical rutile TiO_2 with mesocrystalline structure offered a large specific surface area, mesoporous nature and short transport distance, and thus would promise superior lithium-ion insertion properties. Fig. 3a shows the typical CV curves of the TiO_2-HMs at a scanning rate of 0.5 mVs^{-1} between 1.0-3.0 V. The cathodic peak located at about 1.4 V is attributed to the lithium-ion insertion into the rutile structure, while its associated anodic reaction can be identified as a broad peak at 1.7–2 V. Interestingly, TiO_2-HMs exhibited highly reversible Li storage properties in the voltage window between 0.01-3.0 V (Fig. 3b), which is rarely studied [15]. Fig. 4a and Fig. 4b show the charge-discharge profiles of TiO_2-HMs and commercial rutile TiO_2 nanoparticles (TiO_2-NPs) at 0.1 Ag^{-1} in the voltage windows of 1–3 V. A large reversible capacity of 256 mAh g^{-1} for TiO_2-HMs (89 mAh g^{-1} for TiO_2-NPs) was obtained at the first cycle, indicating a larger storage capacity compared with other rutile TiO_2 nanostructures [14,15]. Moreover, TiO_2-HMs displayed larger Li storage capacity up to 385 mAh g^{-1} at the first charge as well as good reversibility in the voltage window of 0.01-3.0 V, as shown in Fig. 4c. This capacity is much higher than that of TiO_2-NPs (only 145 mAh g^{-1} at the first charge), as shown in Fig. 4d. Thus, the reversible capacity of TiO_2-HMs is larger than that of theoretic value (335 mAh g^{-1}). This could be due to the extra surface capacitance arising from the large specific surface area and mesoporous structure of TiO_2-HMs, corresponding to the CV results. In addition, Super P carbon black may offer some reversible capacity (about 30–50 mAh g^{-1}) according to the previous study [31].

Fig. 4e displays the rate capability of TiO_2-HMs and commercial rutile TiO_2 nanoparticles (TiO_2-NPs) from 0.1 to 2 Ag^{-1} within the

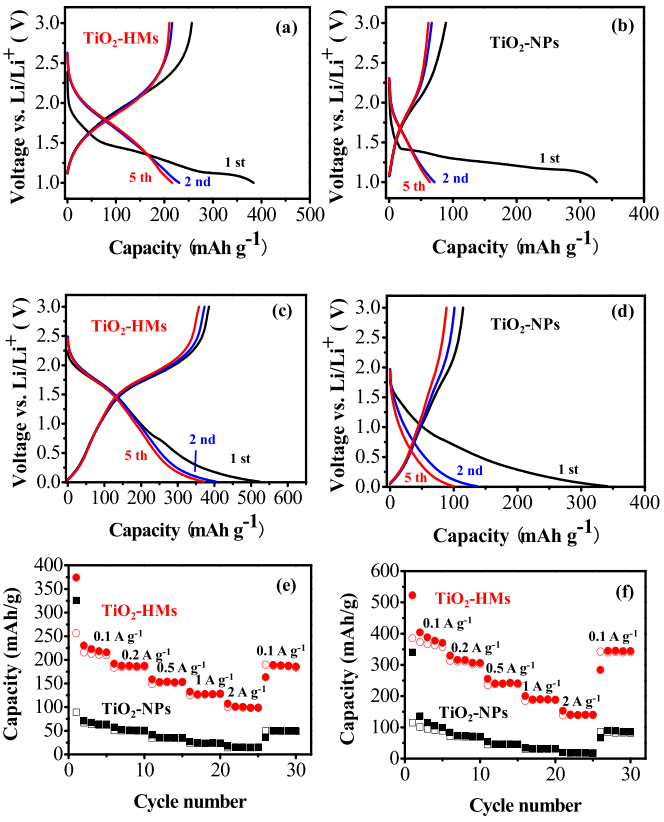

Fig. 4. Li-ion storage properties: charge-discharge profiles of TiO_2-HMs and commercial rutile TiO_2 nanoparticles (TiO_2-NPs) in the voltage windows of (a-b) 1–3 V and (c-d) 0.01–3 V vs. Li/Li^+, rate capability from 0.1-2 Ag^{-1} of TiO_2-HMs and TiO_2-NPs within the voltage windows of (e) 1–3 V and (f) 0.01–3 V vs. Li/Li^+. (filled symbols: discharge capacity and open symbols: charge capacity.).

voltage window of 1–3 V. It could be observed that TiO_2-HMs exhibited superior rate capability, the charge capacity of 212 mAhg^{-1} at 0.1 Ag^{-1} (only 64 mAhg^{-1} for TiO_2-NPs) and 100 mAhg^{-1} at a relatively high rate of 2 Ag^{-1} (less than 15 mAhg^{-1} for TiO_2-NPs) were obtained. In the voltage window of 0.01–3 V (Fig. 4f), TiO_2-HMs displayed a stable capacities of more than 350 mAh g^{-1} at 0.1 Ag^{-1} (about 90 mAh g^{-1} for TiO_2-NPs) and 150 mAh g^{-1} at a high rate of 2 Ag^{-1} (18 mAh g^{-1} for TiO_2-NPs), indicating a good rate performance. Therefore, TiO_2-HMs exhibited remarkably improved lithium-ion storage capacity and rate capability compared with TiO_2-NPs. Besides, it's worth mentioning that the Coulombic efficiency (67%) at the first cycle for TiO_2-HMs is much higher than that of TiO_2-NPs (28%). The improved Li-ion storage properties of TiO_2-HMs could be due to the crystallographically oriented nanostructures providing a large surface area,

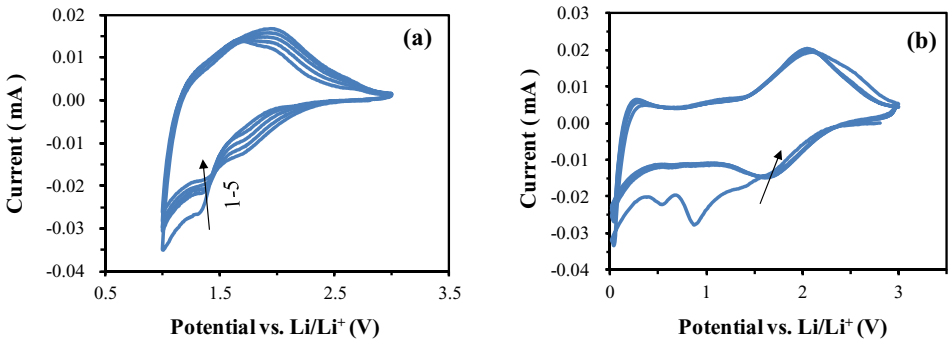

Fig. 3. Cyclic voltammetry curves of TiO_2-HMs in different voltage windows: (a) 1–3 V and (b) 0.01–3 V vs. Li/Li^+.

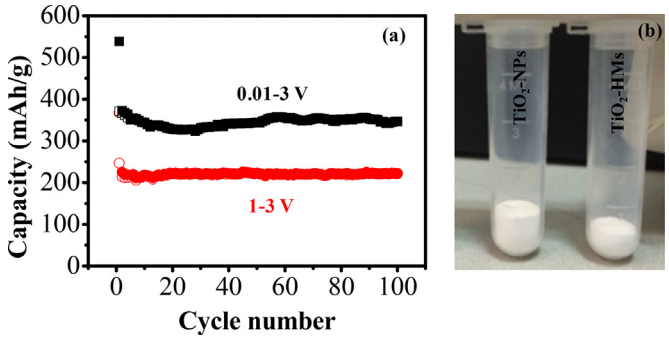

Fig. 5. (a) Cycling stability of TiO_2-HMs for Li-ion storage at 0.1 A g^{-1} in different voltage windows, (b) Comparison of tapped density for TiO_2-HMs and TiO_2-NPs. (Filled symbols: discharge capacity and open symbols: charge capacity.).

nanoporous nature and few grain boundaries between the nanocrystals, which can give more active sites, facilitate the contact between electrode and electrolyte, and also allow the fast electron and ion transport compared to the common nanoparticles.

Fig. 5a shows the cycling stability of TiO_2-HMs for Li-ion storage at 0.1 A g^{-1} in different voltage windows, the stable capacity of 220 mAh g^{-1} and 346 mAh g^{-1} after 100 cycles could be remained within the voltage windows of 1–3 V and 0.01-3.0 V, respectively. This result suggests that TiO_2-HMs demonstrated very good cycling stability. Fig. 5b depicts the volume occupied by the as-prepared TiO_2-HMs, commercial rutile TiO_2 nanoparticles (TiO_2-NPs). Thus, TiO_2-HMs has a higher surface area, but it is worth mentioning that they occupy less volume, leading to a highest tapped density compared to the above two commercial nanopowders. The tapped density of TiO_2-HMs was found to be 1.1 g cm^{-3}, which is more than two times larger compared to TiO_2-NPs (0.53 g cm^{-3}). Therefore, it's well demonstrated here that the hierarchical rutile TiO_2 not only exhibits large storage capabilities, but also significantly high tapped density, and hence possessing high volumetric storage capacity compared to commercially available TiO_2 nanoparticles.

Recently, it was demonstrated that anatase TiO_2 nanostructures could be utilized as potential anode materials for NIBs, and exhibited acceptable capacity and good rate capability [12,32–36]. However, the Na ions insertion behavior of rutile TiO_2 nanocrystals was relatively rarely investigated and its performance urgently needs to be improved [37–39]. Herein, the Na-ion storage properties of the TiO_2-HMs were investigated, and the resutls are shown in Fig. 6. Cyclic voltammetry curves (Fig. 6a) revealed that a couple of redox peaks between around 0.5 V were observed, which could be due to the reversible Ti^{4+}/Ti^{3+} redox [32,38,40].

Fig. 6b and Fig. 6c show the charge-discharge profiles of TiO_2-HMs and TiO_2-NPs from the selective cycles at 0.1 Ag^{-1} in the

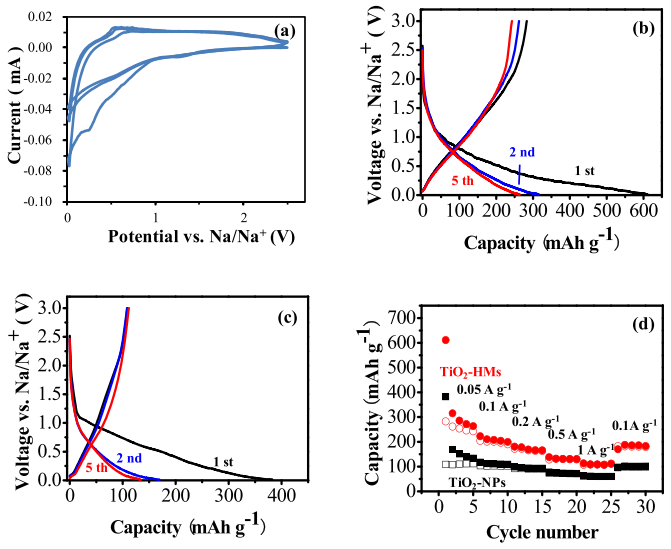

Fig. 6. Na-ion storage properties: (a) Cyclic voltammetry curves of TiO_2-HMs, charge-discharge profiles of (b) TiO_2-HMs and (c) TiO_2-NPs, (d) rate cycling capability from 0.05 to 1 Ag^{-1} of TiO_2-HMs and TiO_2-NPs. (Filled symbols: discharge capacity and open symbols: charge capacity.).

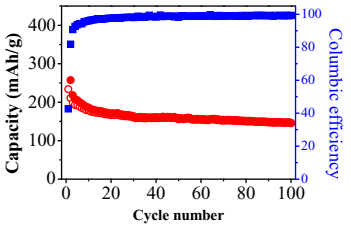

Fig. 7. (a) Cycling stability of TiO_2-HMs for Na-ion storage at 0.1 A g^{-1}.

voltage window of 0.01–3 V. TiO_2-HMs delivered a large discharge capacity of 611 mAh g^{-1} (382 $mAhg^{-1}$ for TiO_2-NPs) and a reversible charge capacity of 283 mAh g^{-1} (only 108 $mAhg^{-1}$ for TiO_2-NPs) were obtained at the first cycle, suggesting a significantly improved Na-ion storage capacity compared with rutile TiO_2 nanoparticles. The low Coulombic efficiency at the first cycle of the TiO_2 electrode may be due to a decomposition reaction in active material [40]. Besides, the conductive carbon may offer about 40 mAh g^{-1} reversible capacity according to the previous report on the Na-ion storage performance of pure Super P [41]. In addition, the Na-ion insertion behavior of rutile TiO_2 is similar to that of anatase TiO_2 from the above results, suggesting that capacitive behavior may have a large effect on the Na-ion storage process in

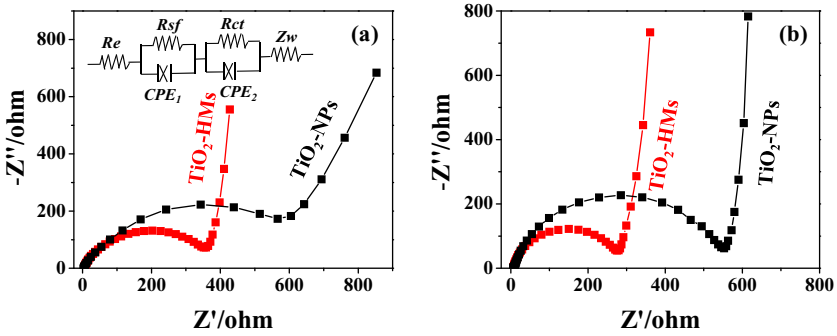

Fig. 8. Electrochemical impedance spectra (EIS) of TiO_2-HMs and TiO_2-NPs using (a) Li and (b) Na metal foil as the reference electrodes. The inset in (a) is the corresponding equivalent circuit.

rutile TiO_2 nanocrystals [32,36,38]. the rutile TiO_2-HMs also exhibited superior rate capability, the charge capacity of 250 mAh g^{-1} at 0.05 Ag^{-1} (70 mAh g^{-1} for TiO_2-NPs) and 110 mAh g^{-1} at a high rate of 1 Ag^{-1} (60 mAh g^{-1} for TiO_2-NPs) were obtained. Fig. 7 shows the cycling stability of TiO_2-HMs for Na-ion storage at 0.1 A g^{-1}, a reversible capacity of 146 mAhg^{-1} could be remained after 100 cycles, indicating a good cycling performance. Moreover, TiO_2-HMs displayed much higher reversible capacity than that of rutile TiO_2 microspheres composed of nanoneedle clusters [38].

In order to investigate the electronic conduction as well as transfer processes of the electrode materials, electrochemical impedance spectroscopy (EIS) has been carried out on the batteries made by TiO_2-HMs and TiO_2-NPs, as shown in Fig. 8. The impedance spectra reveal the internal resistance of the battery: the electrolyte resistance (Re) at high frequencies, a depressed semicircle at the middle frequencies arising from the interface resistance (Rsf) and charge transfer resistance (Rct) and a slope at low frequencies representing the Warburg impedance (W) related to the diffusion process. It could be observed that TiO_2-HMs exhibited much small semicircle both in Li and Na metal foil as the reference electrodes, suggesting remarkably enhanced charge transfer process. The larger slope of the curve (TiO_2-HMs) in Fig. 8a indicates much improved lithium-ions diffusion in the bulk of the active material, which may be due to the tiny size of nanorod subunits (around 5 nm in diameter). However, the low frequency region in EIS for Na and Li sounds different. In the low frequency region (Fig. 8b), typical linear shape of Nyquist plot is observed, but it gradually changes from 45° to 90° with decrease of frequency. This may suggest that the Na-ion storage in rutile TiO_2 is not controlled by the diffusion process [42,43], which further confirm rutile TiO_2 nanocrystals can accommodate Na-ion through surface-induced capacitive processes. Su et al. also demonstrated that the barrier against diffusion of Na ion is not larger during sodiation process in rutile TiO_2 [44]. Thus, it's well demonstrated that the hierarchical rutile TiO_2 constructed by oriented nanorod subunits could make for the fast electron and ion transport compared to the irregularly nanoparticles.

4. Conclusions

In summary, hierarchical rutile TiO_2 with mesocrystalline structure, mesoporous nature and high tapped density was successfully prepared via a one-step, additive-free and facile synthetic route. When the hierarchical rutile TiO_2 with meso-crystalline structure was studied as an anode material for LIBs, it exhibited a high reversible capacity, improved initial Coulombic efficiency, superior rate capability and cycling stability. It's worth mentioning that the hierarchical rutile TiO_2 possesses good Li-ion storage properties under deep cycling conditions (0.01-3.0 V). The hierarchical rutile TiO_2 also demonstrated a large reversible capacity of more than 255 mAh g^{-1} at 0.05 A g^{-1} and good cycling performance. The superior electrochemical storage properties of this material could largely ascribe to the hierarchical architecture with mesoporous nature, larger surface area and highly oriented structure, which could allow the easy access for the electrolyte and provide more active sites. Moreover, the hierarchical TiO_2 exhibited significantly high tapped density hence possessing high volumetric storage capacity compared to commercially available TiO_2 nanoparticles. Therefore, the hierarchical TiO_2 with meso-crystalline structure could be a promising anode material for rechargeable batteries.

Acknowledgements

This work was financially supported by National Natural Science Foundation of China (NSFC 51502038, 21173049 and U1505241), Research Fund for the Doctoral Program of Higher Education of China (RFDP 20133514110002), National Science Foundation of Fujian Province (2015J01042), and Education Department of Fujian Province (JA14081).

References

[1] J.M. Tarascon, M. Armand, Nature 414 (2001) 359–367.
[2] M. Armand, J.M. Tarascon, Nature 451 (2008) 652–657.
[3] L. Croguennec, M.R. Palacin, J. Am. Chem. Soc. 137 (2015) 3140–3156.
[4] H.J. Song, J.-C. Kim, C.W. Lee, S. Park, M.A. Dar, S.-H. Hong, D.-W. Kim, Electrochim. Acta 170 (2015) 25–32.
[5] J.M. Tarascon, Nat. Chem. 2 (2010) 510-510.
[6] N. Yabuuchi, K. Kubota, M. Dahbi, S. Komaba, Chem. Rev. 114 (2014) 11636–11682.
[7] Y. Kim, K.H. Ha, S.M. Oh, K.T. Lee, Chem. Eur. J. 20 (2014) 11980–11992.
[8] M.V. Reddy, G.V. Subba Rao, B.V.R. Chowdari, Chem. Rev. 113 (2013) 5364–5457.
[9] Z. Yang, D. Choi, S. Kerisit, K.M. Rosso, D. Wang, J. Zhang, G. Graff, J. Liu, J. Power Sources 192 (2009) 588–598.
[10] G.-N. Zhu, Y.G. Wang, Y.-Y. Xia, Energy Environ. Sci. 5 (2012) 6652–6667.
[11] Z. Hong, M. Wei, J. Mater. Chem. A 1 (2013) 4403–4414.
[12] R. Massé, E. Uchaker, G. Cao, Sci. China Mater. 58 (2015) 715–766.
[13] G.N. Zhu, C.X. Wang, Y.Y. Xia, J. Electrochem. Soc. 158 (2011) A102.
[14] Y.S. Hu, L. Kienle, Y.G. Guo, J. Maier, Adv. Mater. 18 (2006) 1421–1426.
[15] M. Marinaro, M. Pfanzelt, P. Kubiak, R. Marassi, M. Wohlfahrt-Mehrens, J. Power Sources 196 (2011) 9825–9829.
[16] D.V. Bavykin, J.M. Friedrich, F.C. Walsh, Adv. Mater. 18 (2006) 2807–2824.
[17] P. Roy, S. Berger, P. Schmuki, Angew. Chem. Int. Ed. 50 (2011) 2904–2939.
[18] K. Lee, A. Mazare, P. Schmuki, Chem. Rev. 114 (2014) 9385–9454.
[19] C. Chen, Y. Wen, X. Hu, X. Ji, M. Yan, L. Mai, P. Hu, B. Shan, Y. Huang, Nat. Commun. 6 (2015) 6929.
[20] S. Liu, H. Jia, L. Han, J. Wang, P. Gao, D. Xu, J. Yang, S. Che, Adv. Mater. 24 (2012) 3201–3204.
[21] D. Fattakhova-Rohlfing, A. Zaleska, T. Bein, Chem. Rev. 114 (2014) 9487–9558.
[22] Y. Ren, L.J. Hardwick, P.G. Bruce, Angew. Chem. Int. Ed. 49 (2010) 2570–2574.
[23] H. Cölfen, M. Antonietti, Angew. Chem. Int. Ed. 44 (2005) 5576–5591.
[24] L. Zhou, P. O'Brien, Small 4 (2008) 1566–1574.
[25] R.Q. Song, H. Cölfen, Adv. Mater. 22 (2010) 1301–1330.
[26] E. Uchaker, G. Cao, Nano Today 9 (2014) 499–524.
[27] Z. Hong, M. Wei, J. Chin, Chem. Soc. 62 (2015) 209–216.
[28] M.L. Sushko, K.M. Rosso, J. Liu, J. Phys. Chem. C 114 (2010) 20277–20283.
[29] J. Baek, S. Park, C.K. Song, T.Y. Kim, I. Nam, J.M. Lee, J.W. Han, J. Yi, Chem. Commun. 51 (2015) 15019–15022.
[30] Z. Hong, Y. Xu, Y. Liu, M. Wei, Chem. Eur. J. 18 (2012) 10753–10760.
[31] D. Liu, W. Lei, S. Qin, Y. Chen, Electrochim. Acta 135 (2014) 128–132.
[32] Y. Xu, E. Memarzadeh Lotfabad, H. Wang, B. Farbod, Z. Xu, A. Kohandehghan, D. Mitlin, Chem. Commun. 49 (2013) 8973–8975.
[33] H. Kang, Y. Liu, K. Cao, Y. Zhao, L. Jiao, Y. Wang, H. Yuan, J. Mater. Chem. A 3 (2015) 17899–17913.
[34] K.T. Kim, G. Ali, K.Y. Chung, C.S. Yoon, H. Yashiro, Y.K. Sun, J. Lu, K. Amine, S.T. Myung, Nano Lett. 14 (2014) 416–422.
[35] L. Wu, D. Buchholz, D. Bresser, L. Gomes Chagas, S. Passerini, J. Power Sources 251 (2014) 379–385.
[36] Z. Hong, K. Zhou, Z. Huang, M. Wei, Sci. Rep. 5 (2015) 11960.
[37] H. Usui, S. Yoshioka, K. Wasada, M. Shimizu, H. Sakaguchi, ACS Appl. Mater. Interfaces 7 (2015) 6567–6573.
[38] Y. Zhang, X. Pu, Y. Yang, Y. Zhu, H. Hou, M. Jing, X. Yang, J. Chen, X. Ji, Phys. Chem. Chem. Phys. 17 (2015) 15764–15770.
[39] Z. Hong, K. Zhou, J. Zhang, Z. Huang, M. Wei, J. Mater. Chem. A 3 (2015) 17412–17416.
[40] L. Wu, D. Bresser, D. Buchholz, G.A. Giffin, C.R. Castro, A. Ochel, S. Passerini, Advanced Energy Materials 5 (2015) 1401142.
[41] Y. Cheng, J. Huang, J. Li, Z. Xu, L. Cao, H. Ouyang, J. Yan, H. Qi, J. Alloy. Compd. 658 (2016) 234–240.
[42] Y. Wang, Z. Hong, M. Wei, Y. Xia, Adv. Funct. Mater. 22 (2012) 5185–5193.
[43] A.J. Bard, L.R. Faulkner, Electrochemical Methods Fundamentals and Applications, 2nd ed., John Wiley, Inc, New York, 2001, pp. 233–235.
[44] D. Su, S. Dou, G. Wang, Chem. Mater. 27 (2015) 6022–6029.